Check for updates

Formation of Size-Controllable Tetragonal Nanoprisms by Crystallization-Directed Ionic Self-Assembly of Anionic Porphyrin and PEO-Containing Triblock Cationic Copolymer

Hongjun Jin, Ziyan Wu, Weilin Lin, Yinye Chen, Jingran Zhang, Ruyi Zheng, Haibing Wei, Qinghua Chen, Qingrong Qian,* Jianbin Huang, Jie Zhang,* and Yun Yan**

The creation of anisotropic nanostructures with precise size control is desirable for new properties and functions, but it is challenging for ionic self-assembly (ISA) because of the non-directional electrostatic interactions. Herein, the formation of size-controllable tetragonal nanoprisms is reported via crystallization-directed ionic self-assembly (CDISA) through evaporating a micellar solution on solid substrates. First, ISA is designed with a crystalline polyethylene oxide (PEO) containing cationic polymer poly(2-(2-guanidinoethoxy)ethyl methacrylate)-b-poly(ethyleneoxide)-b-poly(2-(2-guanidinoethoxy)-ethylmethacrylate) (PG_n-PEO_{230}-PG_n) and an anionic 5,10,15,20-Tetrakis(4-sulfonatophenyl) porphyrin (TPPS) to form micelles in aqueous solution. The PG segments binds excessive TPPS with amplenet chargeto form hydrophilic corona, while the PEO segments are unprecedentedly dehydrated and tightly packed into cores. Upon naturally drying the micellar solution on a silicon wafer, PEO crystallizationdirects the micelles to aggregate into square nanoplates, which are further connected to nanoprisms. Length and width of the nanoprisms can be facilely tuned by varying the initial concentration. In this hierarchical process, the aqueous self-assembly is prerequisite and the water evaporation rate is crucial for the formation of nanostructures, which provides multiple factors for morphology regulating. Such precise size-control strategy is highly expected to provide a new vision for the design of advanced materials with size controllable anisotropic nanostructures.

1. Introduction

Molecular self-assembly represents one of the most promising bottom-up methodologies to build well-defined nanostructures across basic science, technology, and nature.[1–4] So far, numerous nanostructures with different morphologies have been created through molecular self-assembly process, such as classic nanospheres,[5,6] 1D nanofibers,[7,8] 2D platelets[9,10] and various hierarchical structures.[11,12] Above all, anisotropic nanostructures have been actively investigated due to the increasing recognition that anisotropic shape and size at nanoscale has a significant effect on material properties and functionality.[13–15] In nature, hierarchical self-assembly and crystallization with long-range orientation and ordered spatial arrangement is a ubiquitous pathway to regulate structures and biological functions.[16] Inspired by the crystallographic regulation in biology, extensive effort has been exerted to build anisotropic nanostructures and precisely regulate the shape and size by crystallization kinetics control. Pioneering works discovered by Manners and co-workers have revealed that by introducing a crystallizable core-forming chain to block copolymers (BCP), the obtained crystalline BCPs can assemble into 1D or 2D nanostructures with controlled morphologies through an epitaxial crystallization process.[9,17–21] Over the past two decades, such a strategy has been widely applied for controlling the size and shape of crystalline BCPs.[22–26] Liquid crystalline block copolymers also attract much attention

H. Jin, Z. Wu, W. Lin, Y. Chen, J. Zhang, Q. Chen, Q. Qian
Engineering Research Center of Polymer Green Recycling of
Ministry of Education
College of Environmental and Resource Sciences
College of Carbon Neutral Modern Industry
Fujian Normal University
Fuzhou, Fujian 350117, China
E-mail: qrqian@fjnu.edu.cn

The ORCID identification number(s) for the author(s) of this article can be found under https://doi.org/10.1002/smll.202300688.

DOI: 10.1002/smll.202300688

H. Jin, R. Zheng, H. Wei, J. Huang, J. Zhang, Y. Yan
Beijing National Laboratory for Molecular Sciences (BNLMS)
College of Chemistry and Molecular Engineering
Peking University
Beijing 100871, China
E-mail: hbwei@hfut.edu.cn; jz10@pku.edu.cn; yunyan@pku.edu.cn

H. Wei
Department of Polymer Science and Engineering
School of Chemistry and Chemical Engineering
Hefei University of Technology
Hefei 230009, China

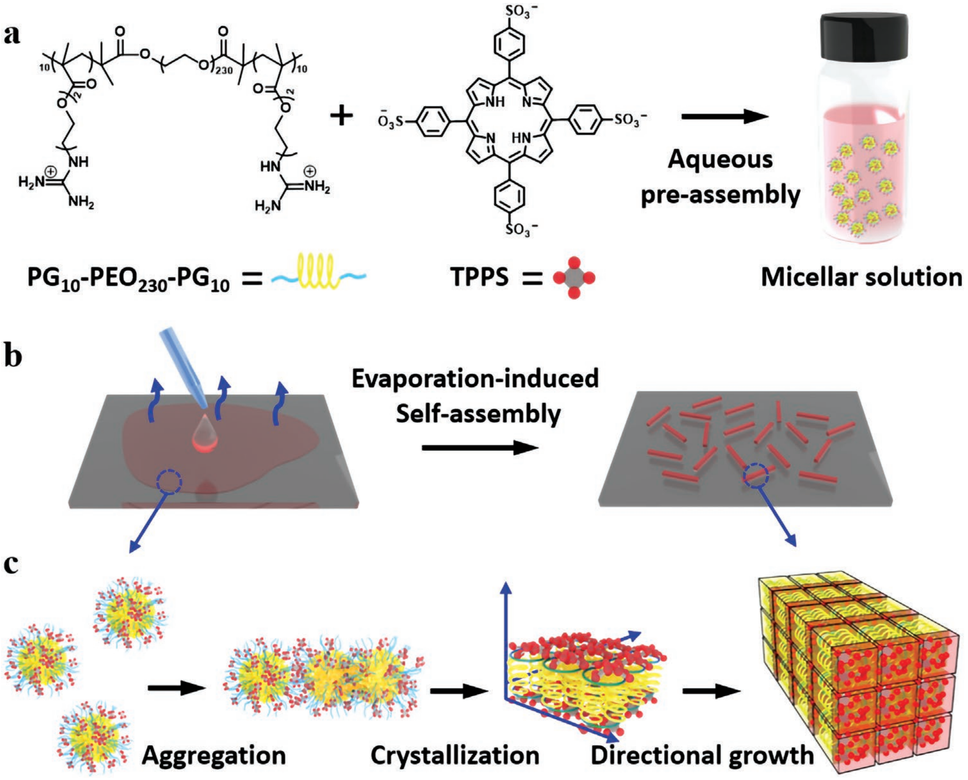

Scheme 1. Illustration of the crystallization-directed ionic self-assembly process, which involves a) the aqueous pre-assembly of PG$_{10}$-PEO$_{230}$-PG$_{10}$ and TPPS to form micelles in aqueous solution and b) the subsequent evaporation-induced self-assembly on substrate to form well-defined tetragonal nanoprisms. c) The proposed mechanism of the evaporation-induced self-assembly.

to fabricate and regulate anisotropic nanostructures, especially in the condensed state of matter.[27–29] Besides, some recent works reveal that small organic molecules also display controllable anisotropic morphologies and length distribution by rationally designing the directional noncovalent interactions, such as hydrogen bonding and π–π stacking,[30–35] which provided a broader insight into the design of controllable self-assembly and supramolecular materials. However, so far, it remains challenging to create size-controllable anisotropic nanostructures via ionic self-assembly (ISA), because the electrostatic interactions are isotropic, which greatly impedes directional growth.[36]

Over time, electrostatic interactions have been extensively employed to build ISA where intriguing functions and properties can originate from the versatile combinations of the oppositely charged pairs.[37–39] However, for a given composition of positively and negatively charged species, the size distribution of the ionic self-assembled nanostructures is usually unchanged with variation of concentration, but the number of the nanostructures is proportional to the overall concentration.[40] Inspired by the directional crystallization, we proposed that introducing crystalline component into ionic system may provide a self-assembling orientation to form anisotropic nanostructures. Thus, in this work, we synthesized a crystalline polyethylene oxide (PEO) containing ABA type triblock cationic polymer poly(2-(2-guanidinoethoxy)ethyl methacrylate)-b-poly(ethyleneoxide)-b-poly(2-(2-guanidinoethoxy)-ethylmethacrylate)PG$_{10}$-PEO$_{230}$-PG$_{10}$ and the ISA was designed to build with an anionic 5,10,15,20-Tetrakis(4-sulfonatophenyl) porphyrin (TPPS). In contrast to the controllable self-assembly of most crystalline BCPs which generally occurs in selective solvents, the precise size control of well-defined nanostructures on surfaces attracts increased attention owing to the significant importance in the areas of lithography, superhydrophobicity, and cell adhesion.[41–45] Crystalline polymers such as PEO and polycaprolactone (PCL) were recently reported to form nanocubes by evaporation-induced crystallization on surfaces.[46–48] However, the crystallization shows little effect on growth orientation, leading to the failure of shape and size regulation.

Herein, we report an exquisite crystallization-directed ionic self-assembly (CDISA) to build size-controllable tetragonal nanoprisms via aqueous ISA of PG$_{10}$-PEO$_{230}$-PG$_{10}$ and TPPS followed by an evaporation-induced aggregation (**Scheme 1**). Through the aqueous ISA process, PG$_{10}$-PEO$_{230}$-PG$_{10}$ and TPPS form an unwonted micellar structure, in which the PG/TPPS parts form coronas while the PEO segments form cores, because the PG/TPPS ends combined with excessive TPPS with ample net charge while the PEO segments are dehydrated and tightly packed in the micelles. The aqueous self-assembly is a prerequisite for the formation of nanoprisms. Then, upon naturally drying the micellar solution on solid substrates such as silicon wafer, the crystallization of PEO directs the micelles to aggregate into square nanoplates, which are ulteriorly connected by the active PG/TPPS ends to form well-defined tetragonal nanoprisms. Remarkably, the length and width of the obtained nanoprisms can be readily tuned by varying the initial concentration of the micellar solution. Further study reveals that crystallization kinetics plays a crucial role in the formation of the nanoprisms, which allows multiple factors for morphology regulation, such as temperature, relative humidity (RH), and drying method. We envision the current work will map out a new vista in the anisotropic ISA of nanostructures with precise chemistries on material surfaces.

2. Results and Discussion

Aqueous ISA was constructed by mixing the solutions of the anionic 5,10,15,20-Tetrakis(4-sulfonatophenyl) porphyrin (TPPS) and the synthesized cationic ABA type triblock copolymer poly(2-(2-guanidinoethoxy)ethyl methacrylate)-b-poly(ethyleneoxide)-b-poly(2-(2-guanidinoethoxy)-ethylmethacrylate) (PG_n-PEO_{230}-PG_n) followed by storing at 25 °C for 24 h. PG_n-PEO_{230}-PG_n has two short cationic PG segments (n ≈ 10, calculated from ^1H NMR, Figure S1, Supporting Information) tethered by a long PEO chain with 230 EO units which were synthesized according to our previous work.[49] Cryogenic transmission electron microscopy (Cryo-TEM) shows that TPPS and PG_{10}-PEO_{230}-PG_{10} self-assembles into spherical micelles and partially fused into rod-like micelles with a diameter of ≈10–20 nm at a charge balancing ratio of [+]:[–] = 4 mM:4 mM (**Figure 1**a, inset: Tyndall effect of the mixed solution). Variation in concentration barely affects the micellar shape and size

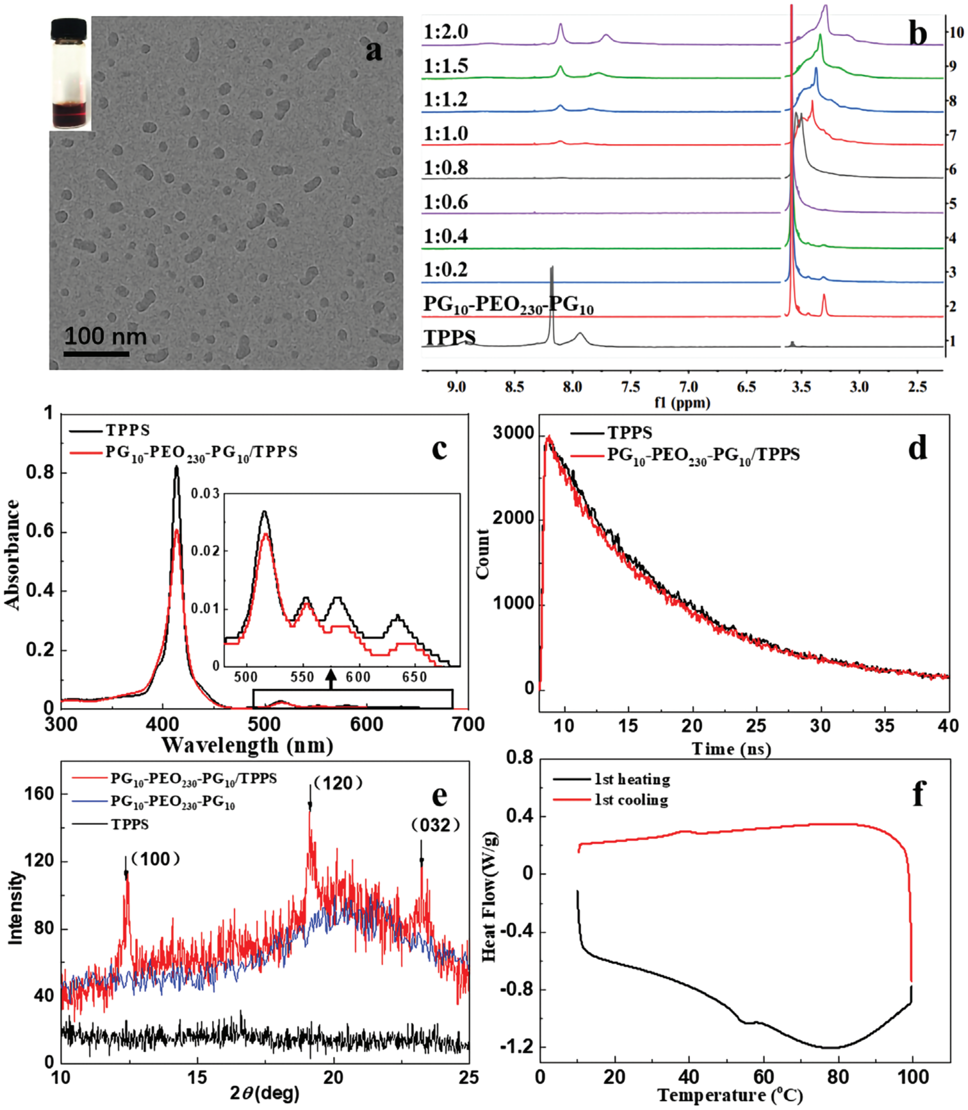

Figure 1. a) Cryo-TEM image of the PG_{10}-PEO_{230}-PG_{10}/TPPS micelles ([+]:[–] = 1:1, [TPPS] = 1 mM). Inset shows the Tyndall effect of the mixed solution. b) ^1H NMR (600 MHz, D_2O) spectra of TPPS ([–] = 4 mM), PG_{10}-PEO_{230}-PG_{10} ([+] = 4 mM) and PG_{10}-PEO_{230}-PG_{10}/TPPS at different charge ratio from [+]:[–] = 1:0.2 to 1:2.0 with a fixed [+] = 4 mM, respectively. c) UV–vis spectra and d) transient absorption spectra of the TPPS solution (black line) and the micellar solution (red line), respectively ([TPPS] = 0.05 mM). e) XRD patterns of the PG_{10}-PEO_{230}-PG_{10}/TPPS precipitates collected from the aqueous solution after storing for 5 days ([+]:[–] = 1:1, [TPPS] = 2.5 mM), freeze-dried PG_{10}-PEO_{230}-PG_{10} and TPPS samples, respectively. f) DSC curves of the PG_{10}-PEO_{230}-PG_{10}/TPPS precipitates.

(Figure S2, Supporting Information). It is well-known that PEO or PEG containing amphiphilic block copolymers in aqueous solution generally form flower-like micelles with an amorphous PEO or PEG coronary shell due to its hydrophilic nature.[49–51] Herein, it is very interesting to find that the PEO segments are dehydrated and tightly packed to form inner cores of the micelles while the PG/TPPS ends with excessive TPPS form the hydrophilic shell.

Figure 1b shows the ^{1}H nuclear magnetic resonance (^{1}H NMR) spectra of the TPPS, PG_{10}-PEO_{230}-PG_{10}, and PG_{10}-PEO_{230}-PG_{10}/TPPS solutions at different charge ratio from [+]:[–] = 1:0.2 to 1:2.0. As the ratio of TPPS increasing, the peak at $\delta = 3.36$ ppm for CH_2-N of PG_{10}-PEO_{230}-PG_{10} gradually decreases, indicating the occurrence of electrostatic interactions between TPPS and PG. The chemical shift of EO-CH_2 group at $\delta = 3.60$ ppm displays a notable upfield shift with the increasing of TPPS, suggesting the local environment of PEO segments is significantly changed. Since the chemical shift of EO-CH_2 group shifts downfield in water due to the deshielding effect resulting from interactions between EO-CH_2 protons and water.[52] Thus, the PEO segments in PG_{10}-PEO_{230}-PG_{10}/TPPS micelles are apparently dehydrated and form a relatively hydrophobic microenvironment. Furthermore, as it is known that the half-height width $\Delta\nu_{1/2}$ is inversely proportional to T_2, which is a measure of the mobility of the related segments.[52,53] The significant peak broadening and $\Delta\nu_{1/2}$ increasing of the EO-CH_2 signal reveals the dramatic decrease in mobility of the PEO segments, indicating their tight packing in the confined micelles. Meanwhile, the considerable negative Zeta potential (-25.48 mV) and the appearance of TPPS ^{1}H signal in the [+]:[–] = 1:1 micellar system (Figure 1b), indicating the formation of TPPS shell around the dehydrated PEO rather than the inverse model.[54] Besides, the tightly packed PEO chains can be probably observed under Cryo-TEM due to high electron density. Thus, if PEO chains formed corona (the thickness is estimated ≈10 nm[46,54]), dinamiter of the micelles should be obviously greater than 10–20 nm. Furthermore, because the PEO chain can bind Li^+,[55,56] we use LiI to make PEO easier to be observed. Li^+ was successfully loaded as the ^{1}H NMR and 2D DOSY spectra illustrated (Figure S3a–c, Supporting Information). However, the diameter of the LiI loaded micelles was still ≈10-20 nm (Figure S3d, Supporting Information). Thus, the PEO chains formed cores rather than corona.

UV–vis absorption spectra show the characteristic Soret band and Q bands of TPPS barely shift upon the formation of micelles (Figure 1c). Both transient absorption spectra of the TPPS solution and micellar solution display single exponential decay and the fluorescence lifetime slightly decreases from 10.00 ns to 9.63 nm (Figure 1d). Thus, the TPPS molecules arrange disorderly as monomer in the micellar shell without any H or J-aggregates,[54] which makes the TPPS molecules very dynamic. Owing to the thermodynamic instability of the colloidal micelles, when the initial concentration increases to 2.5 mᴍ, the PG_{10}-PEO_{230}-PG_{10}/TPPS micelles gradually flocculate to form precipitates after storing for 5 days. X-ray diffraction (XRD) patterns suggest the PEO segments partially crystalize into an ordered arrangement in the precipitates (Figure 1e).[57–59] Differential scanning calorimetry (DSC) curves show an endothermic melting peak at 55.8 °C and an exothermic crystallization peak at 38.2 °C in the first heating and cooling scans, respectively (Figure 1f), which is well consistent with the thermal behavior of pure crystalline PEO. The crystallinity is ≈1.1%, which is calculated with the first cycle melting enthalpy. However, despite the PEO segments crystalize, the micelles fail to form well-defined anisotropic nanostructures through the solution self-assembly process (Figure S4, Supporting Information).

To obtain anisotropic nanostructures, evaporation-induced self-assembly was then conducted. We observed that upon depositing the micellar solution ([+]:[–] = 1:1, [TPPS] = 0.5 mᴍ) on various solid substrates and then drying naturally in an incubator at 25 °C under RH of ≈20%, it spontaneously forms well-defined tetragonal nanoprisms as the scanning electron microscopy (SEM) and transmission electron microscopy (TEM) images show in **Figure 2**a,b and Figure S5 (Supporting Information). Large scale SEM image displayed that most of the aggregates were nanoprisms (Figure S6, Supporting Information), which indicated a high yield. XPS results (Table S1 and Figure S7, Supporting Information) showed that the measured atomic percent (At%) of N (4.35%) and S (1.38%) were only a little lower than the theoretical values, which are 6.06% and 1.51%, respectively, indicating the PG/TPPS ends are not wrapped in the thick PEO chains. The counterions of CF_3COO- and Na^+ were evenly distributed on the nanoprisms as the SEM-EDX mapping showed (Figure S8, Supporting Information). However, when too many extra salts were added such as LiI (LiI:TPPS = 200:1), distinctive salt crystals were observed (Figure S9, Supporting Information). XRD and DSC measurements suggest the PEO segments crystalize into periodic arrangement with a significantly improved crystallinity to 10.1% in the nanoprisms (Figure 2c,d). Thus, the evaporation-induced self-assembly greatly facilitates the crystallization of PEO. Moreover, it is remarkable that the size of the nanoprisms is significantly affected by the initial concentration of the micellar solution. When the concentration decreases to 0.05 mᴍ, tetragonal nanoplates with a thickness of ≈30–40 nm were formed (Figure 2e–f). Conventionally, polymer chains fold back and forth into stems to form crystalline lamellae with a thickness of ≈10–20 nm.[60,61] Thus, we proposed that via evaporation-induced self-assembly, the PG_{10}-PEO_{230}-PG_{10}/TPPS micelles aggregate and crystalize to form tetragonal lamellae. The directional crystallization of PEO chains result in more active ends of PG/TPPS distributed on the horizontal plane of lamellae which leads to greater growth rate in the vertical direction than that in the horizontal direction. Thus, connected by the active ends with dynamic ionic interactions, the tetragonal lamellae grow directionally into anisotropic nanoprisms (Scheme 1).

To further support the hierarchical self-assembly mechanism, equal volume (2 µL) of the micellar solutions with different concentrations were dried through the same process. **Figure 3**a–c and Figure S10 (Supporting Information) show that all the samples form well-defined nanoprisms and the size of the nanoprisms increases with the increasing concentrations. The length and width distributions (from 100 samples) are statistically shown in Figure 3d,e. Notably, the average length and width increase linearly with the concentration (Figure 3f,g).

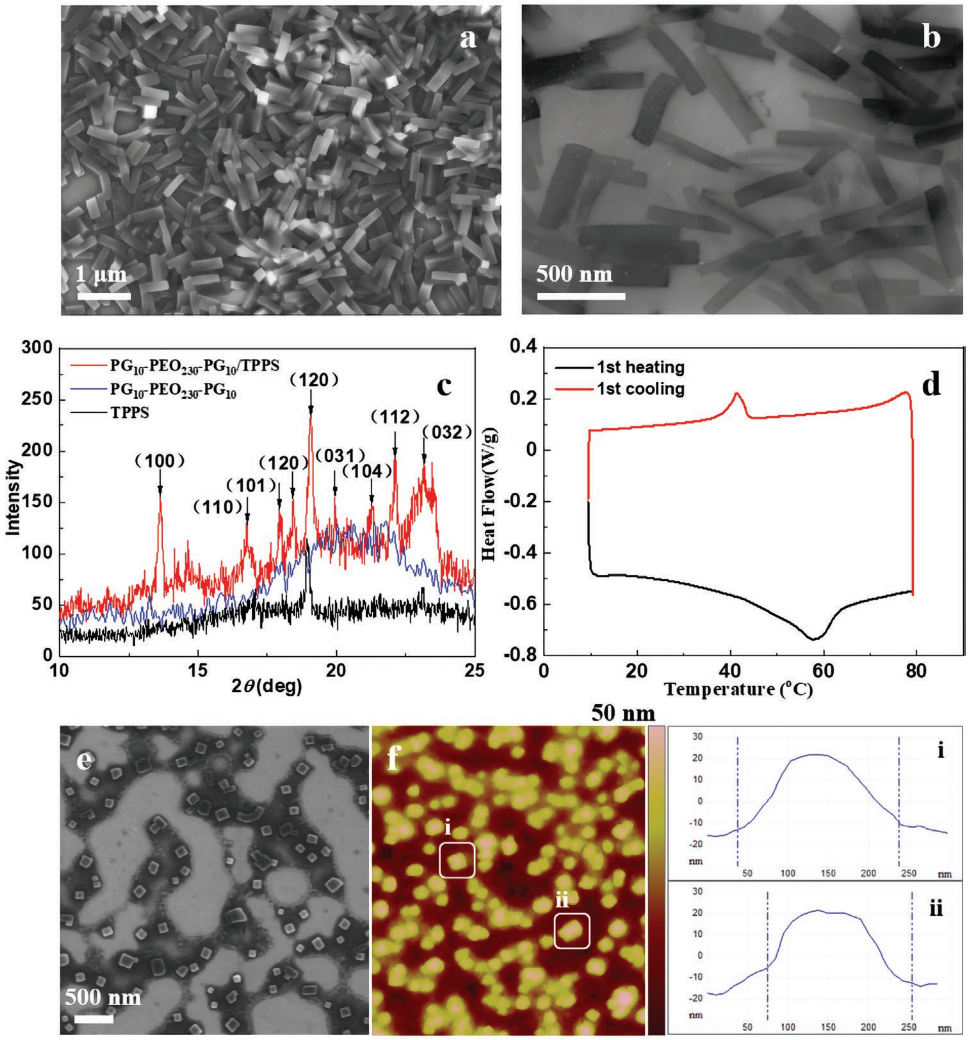

Figure 2. a) SEM and b) TEM image of the nanoprisms formed on (a) silicon wafer and (b) copper grids coated with Formvar film through evaporating the PG$_{10}$-PEO$_{230}$-PG$_{10}$/TPPS solution ([TPPS] = 0.5 mм, [+]:[–] = 1:1) at 25 °C in the incubator. c) XRD pattern and d) DSC curves of the PG$_{10}$-PEO$_{230}$-PG$_{10}$/TPPS nanoprisms collected from the silicon wafer. e) SEM and f) atomic force microscopy (AFM) image of the nanoplates formed on silicon wafer through evaporating the PG$_{10}$-PEO$_{230}$-PG$_{10}$/TPPS solution ([TPPS] = 0.05 mм, [+]:[–] = 1:1).

Moreover, when the micellar solutions are pre-stored at 4 °C for 24 h, the obtained nanoprisms display narrower size distribution through the same drying process at 25 °C (Figure 3h–j; Figure S11, Supporting Information), indicating the aqueous pre-assembly may play an important role in the formation of nanoprisms.

To understand the effect of the pre-assembly, control experiments were conducted. Different from the micellar solution, neither TPPS nor PG$_{10}$-PEO$_{230}$-PG$_{10}$ solution could form nanoprisms through the same process (Figure S12, Supporting Information). Then, we replaced TPPS with 1,3-benzenedisulfonic acid sodium (BDSS). PG$_{10}$-PEO$_{230}$-PG$_{10}$/BDSS solutions ([BDSS] = 1 mм, [+]:[–] = 1:1) were prepared at 25 and 4 °C, respectively. The PG$_{10}$-PEO$_{230}$-PG$_{10}$/BDSS solution stored at 25 °C for 24 h shows no obvious Tyndall effect (**Figure 4**a inset), indicating few aggregates were formed. Evaporating through the routine process, well-defined nanostructures were barely obtained (Figure 4a). In contrast, when the solution was stored at 4 °C for 8 h and 24 h, aqueous self-assembly occurred with a distinct Tyndall effect and nanoprisms were gradually formed after drying (Figure 4b,c). Therefore, the aqueous self-assembly is clearly a prerequisite for the formation of well-defined nanoprisms.

Furthermore, water evaporation rate has an essential effect on the morphologies of the obtained nanostructures. Rapid evaporation by freeze-drying and room-temperature vacuum drying lead to interconnected irregular structures (Figure S13, Supporting Information), due to the deficient chain rearrangement and crystallization. Meanwhile, when the evaporating rate is accelerated by heating at 50–300 °C, the obtained nanostructures gradually become irregular and isotropic (Figure 4d–f), which is mainly resulted from the lack of assembly orientation by PEO crystallization. In order to fine-tune the evaporation rate, the micellar solutions were dried under controlled relative humidity (RH = 0, 11, 21, 57, 75, and 98%) at room temperature.[62] Rapid evaporating rate under extremely dry

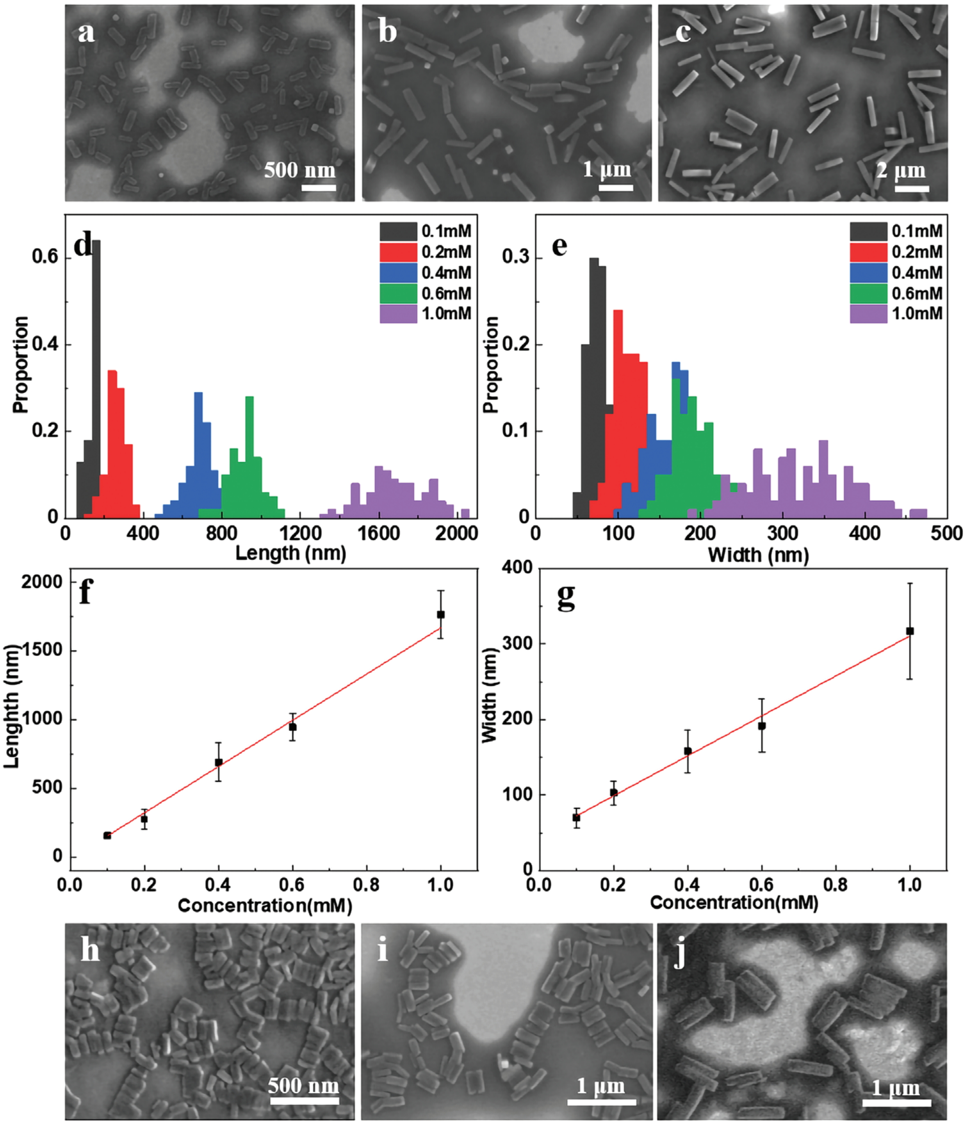

Figure 3. a–c) SEM images of the nanoprisms formed from evaporating the PG_{10}-PEO_{230}-PG_{10}/TPPS solutions prepared at 25 °C with different concentrations of 0.2, 0.6, and 1.0 mm, respectively. d) Length and e) width distribution of the nanoprisms. The linear relationship between the solution concentration and the f) length and g) width. h–j) SEM images of the nanoprisms formed from evaporating the PG_{10}-PEO_{230}-PG_{10}/TPPS solutions prepared at 4 °C with different concentrations of 0.2, 0.4, and 0.6 mm, respectively.

conditions (RH = 0 and 11%) also leads to irregular morphologies (Figure S14a,b, Supporting Information). Under common ambient conditions with RH of 21–75%, well-defined nanofibers were consistently formed and the length significantly increases with the increasing RH (Figure 4g–i). However, extreme high RH of 98% with a very low evaporating rate causes irregular structure as well (Figure S14c, Supporting Information). Thus, the crystallization kinetics plays a crucial role in the formation of nanostructures.

3. Conclusion

In summary, we demonstrated a novel crystallization-directed ionic self-assembly (CDISA) to create well-defined anisotropic nanoprisms with precise controlled size via an aqueous pre-assembly and a subsequent evaporating-induced crystallization. The pre-assembly of PG_{10}-PEO_{230}-PG_{10} and TPPS forms confined micelles with an unprecedented dehydrated and tightly packed PEO core and a dynamic PG/TPPS shell, which provides a prerequisite for the formation of nanoprisms. Upon drying on substrates, the micelles gradually connect and bundle together to form well-defined tetragonal nanoprisms directed by the PEO crystallization. The length and width of the obtained nanoprisms are linearly related to the concentration of micellar solution, which further supports the hierarchical self-assembly process. The key factor for the formation and size control of the nanoprisms owes to crystallization kinetics which can be finely controlled by regulating the water evaporation rate. While the general applicability of the CDISA merit further

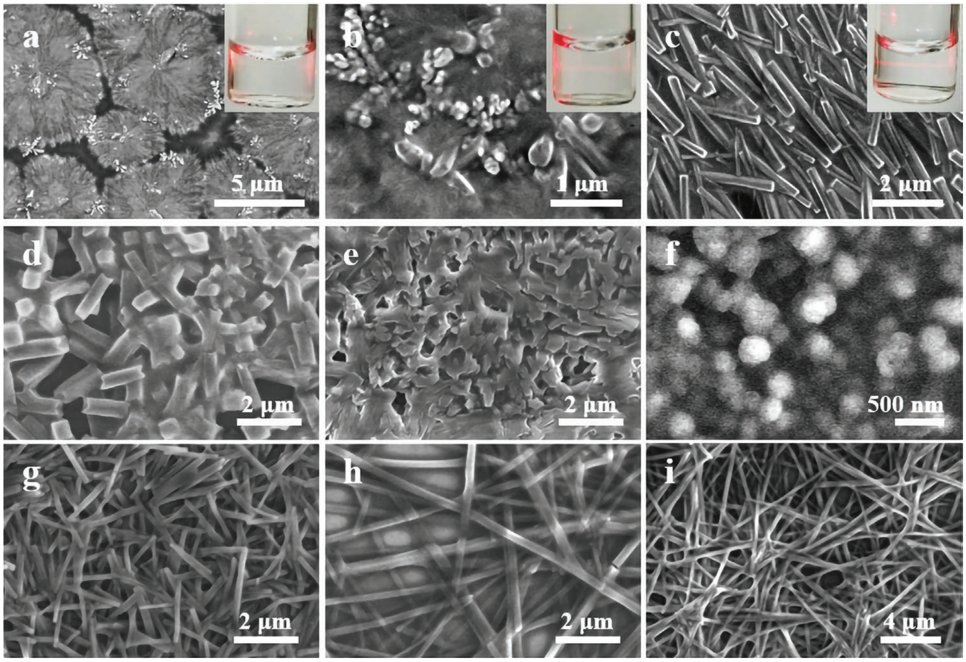

Figure 4. SEM images of the morphologies formed from evaporating the PG$_{10}$-PEO$_{230}$-PG$_{10}$/BDSS solutions stored at a) 25 °C for 24 h, b) 4 °C for 8 h, and c) 4 °C for 24 h. Insets show the corresponding Tyndall effect. SEM images of the nanostructures formed from evaporating the PG$_{10}$-PEO$_{230}$-PG$_{10}$/TPPS solutions by air drying at d) 50 °C, e) 200 °C, f) 300 °C. SEM images of the nanostructures formed from evaporating the PG$_{10}$-PEO$_{230}$-PG$_{10}$/TPPS solutions by air drying under controlled RH of g) 21%, h) 57%, and i) 75%, respectively, at room temperature.

investigation, we expect this work may provide insight in the creation of size-controllable anisotropic nanostructures through ionic self-assembly.

Supporting Information

Supporting Information is available from the Wiley Online Library or from the author.

Acknowledgements

This work was supported financially by the National Natural Science Foundation of China (NSFC 22202044, 22172004, and 21404030).

Conflict of Interest

The authors declare no conflict of interest.

Data Availability Statement

The data that support the findings of this study are available from the corresponding author upon reasonable request.

Keywords

anisotropic nanostructures, crystallization, ionic self-assembly, size control, triblock copolymers

Received: February 1, 2023
Revised: March 5, 2023

---

[1] R. Service, *Science* **2005**, *309*, 95.
[2] Y. Gao, J. Shi, D. Yuan, B. Xu, *Nat. Commun.* **2012**, *3*, 1033.
[3] L. Jiang, W. de Folter, J. Huang, A. Philipse, W. Kegel, A. Petukhov, *Angew. Chem., Int. Ed.* **2013**, *52*, 3364.
[4] J. Gao, J. Zhan, Z. Yang, *Adv. Mater.* **2020**, *32*, 1805798.
[5] S. Li, Q. Zou, Y. Li, C. Yuan, R. Xing, X. Yan, *J. Am. Chem. Soc.* **2018**, *140*, 10794.
[6] L. Shi, F. Hu, Y. Duan, W. Wu, J. Dong, X. Meng, X. Zhu, B. Liu, *ACS Nano* **2020**, *14*, 2183.
[7] J. Zhan, Y. Cai, S. He, L. Wang, Z. Yang, *Angew. Chem., Int. Ed.* **2018**, *57*, 1813.
[8] F. Ding, H. Deng, Y. Du, X. Shi, Q. Wang, *Nanoscale* **2014**, *6*, 9477.
[9] Z. Hudson, C. Boott, M. Robinson, P. Rupar, M. Winnik, I. Manners, *Nat. Chem.* **2014**, *6*, 893.
[10] B. Liu, Y. Yao, S. Che, *Angew. Chem., Int. Ed.* **2013**, *52*, 14186.
[11] Y. Lu, J. Lin, L. Wang, L. Zhang, C. Cai, *Chem. Rev.* **2020**, *120*, 4111.
[12] L. Huang, Z. Lei, T. Huang, Y. Zhou, Y. Bai, *Nanoscale* **2017**, *9*, 2145.
[13] A. Pearce, T. Wilks, M. Arno, R. O'Reilly, *Nat. Rev. Chem.* **2020**, *5*, 21.
[14] K. Thorkelsson, P. Bai, T. Xu, *Nano Today* **2015**, *10*, 48.
[15] S. Sacanna, D. Pine, *Curr. Opin. Colloid Interface Sci.* **2011**, *16*, 96.
[16] C. Yuan, W. Ji, R. Xing, J. Li, E. Gazit, X. Yan, *Nat. Rev. Chem.* **2019**, *3*, 567.
[17] X. Wang, G. Guerin, H. Wang, Y. Wang, I. Manners, M. Winnik, *Science* **2007**, *317*, 644.
[18] P. Rupar, L. Chabanne, M. Winnik, I. Manners, *Science* **2012**, *337*, 559.

[19] A. Soto, J. Gilroy, M. Winnik, I. Manners, *Angew. Chem., Int. Ed.* **2010**, *49*, 8220.
[20] R. Hailes, A. Oliver, J. Gwyther, G. Whittell, I. Manners, *Chem. Soc. Rev.* **2016**, *45*, 5358.
[21] L. MacFarlane, C. Zhao, J. Cai, H. Qiu, I. Manners, *Chem. Sci.* **2021**, *12*, 4661.
[22] M. Inam, G. Cambridge, A. Pitto-Barry, Z. Laker, N. Wilson, R. Mathers, A. Dove, R. O'Reilly, *Chem. Sci.* **2017**, *8*, 4223.
[23] N. Petzetakis, A. Dove, R. O'Reilly, *Chem. Sci.* **2011**, *2*, 955.
[24] W. Yu, J. Foster, A. Dove, R. O'Reilly, *Macromolecules* **2020**, *53*, 1514.
[25] L. Beun, L. Albertazzi, D. van der Zwaag, R. de Vries, M. Cohen Stuart, *ACS Nano* **2016**, *10*, 4973.
[26] J. Schmelz, M. Karg, T. Hellweg, H. Schmalz, *ACS Nano* **2011**, *5*, 9523.
[27] H. Yu, *Prog. Polym. Sci.* **2014**, *39*, 781.
[28] T. Gao, X. Wang, L. Yang, H. He, X. Ba, J. Zhao, F. Jiang, *ACS Appl. Mater. Interfaces* **2017**, *9*, 24846.
[29] S. Huang, Y. Chen, S. Ma, H. Yu, *Angew. Chem., Int. Ed.* **2018**, *130*, 12704.
[30] S. Ogi, K. Sugiyasu, S. Manna, S. Samitsu, M. Takeuchi, *Nat. Chem.* **2014**, *6*, 188.
[31] S. Ogi, V. Stepanenko, K. Sugiyasu, M. Takeuchi, F. Wurthner, *J. Am. Chem. Soc.* **2015**, *137*, 3300.
[32] D. van der Zwaag, T. de Greef, E. Meijer, *Angew. Chem., Int. Ed.* **2015**, *54*, 8334.
[33] J. Kang, D. Miyajima, T. Mori, Y. Inoue, Y. Itoh, T. Aida, *Science* **2015**, *347*, 646.
[34] T. Fukui, S. Kawai, S. Fujinuma, Y. Matsushita, T. Yasuda, T. Sakurai, S. Seki, M. Takeuchi, K. Sugiyasu, *Nat. Chem.* **2017**, *9*, 493.
[35] M. Wehner, F. Würthner, *Nat. Rev. Chem.* **2019**, *4*, 38.
[36] L. Xu, L. Jiang, M. Drechsler, Y. Sun, Z. Liu, J. Huang, B. Tang, Z. Li, M. Stuart, Y. Yan, *J. Am. Chem. Soc.* **2014**, *136*, 1942.
[37] A. Harada, K. Kataoka, *Science* **1999**, *283*, 65.
[38] H. Jin, M. Xie, W. Wang, L. Jiang, W. Chang, Y. Sun, L. Xu, S. Zang, J. Huang, Y. Yan, L. Jiang, *CCS Chem.* **2020**, *2*, 98.
[39] H. Jin, C. Ma, W. Wang, Y. Cai, J. Qi, T. Wu, P. Liao, H. Li, Q. Zeng, M. Xie, J. Huang, Y. Yan, *ACS Mater. Lett.* **2021**, *4*, 145.
[40] Y. Yan, N. Besseling, A. de Keizer, A. Marcelis, M. Drechsler, M. Cohen Stuart, *Angew. Chem., Int. Ed.* **2007**, *46*, 1807.
[41] J. Cai, C. Li, N. Kong, Y. Lu, G. Lin, X. Wang, Y. Yao, I. Manners, H. Qiu, *Science* **2019**, *366*, 1095.
[42] O. El-Zubir, E. Kynaston, J. Gwyther, A. Nazemi, O. Gould, G. Whittell, B. Horrocks, I. Manners, A. Houlton, *Chem. Sci.* **2020**, *11*, 6222.
[43] Z. Tang, L. Gao, J. Lin, C. Cai, Y. Yao, G. Guerin, X. Tian, S. Lin, *J. Am. Chem. Soc.* **2021**, *143*, 14684.
[44] T. Hai, Z. Feng, Y. Sun, W. Wong, Y. Liang, Q. Zhang, Y. Lei, *ACS Nano* **2022**, *16*, 3290.
[45] R. Harniman, S. Pearce, I. Manners, *J. Am. Chem. Soc.* **2022**, *144*, 951.
[46] K. Margulis, X. Zhang, L. Joubert, K. Bruening, C. Tassone, R. Zare, R. Waymouth, *Angew. Chem., Int. Ed.* **2017**, *56*, 16357.
[47] S. Tu, B. Wang, Y. Chen, Z. Li, X. Luo, *ACS Macro Lett.* **2012**, *1*, 933.
[48] W. Zhang, L. Shi, Y. An, X. Shen, Y. Guo, L. Gao, Z. Liu, B. He, *Langmuir* **2003**, *19*, 6026.
[49] H. Wei, S. Du, Y. Liu, H. Zhao, C. Chen, Z. Li, J. Lin, Y. Zhang, J. Zhang, X. Wan, *Chem. Commun.* **2014**, *50*, 1447.
[50] A. Harnoy, I. Rosenbaum, E. Tirosh, Y. Ebenstein, R. Shaharabani, R. Beck, R. Amir, *J. Am. Chem. Soc.* **2014**, *136*, 7531.
[51] L. Zhao, R. Ma, J. Li, Y. Li, Y. An, L. Shi, *Biomacromolecules* **2008**, *9*, 2601.
[52] J. Ma, C. Guo, Y. Tang, H. Liu, *Langmuir* **2007**, *23*, 9596.
[53] J. Ma, Y. Tang, J. Xiang, S. Chen, J. Wang, H. Liu, *J. Colloid Interf. Sci.* **2007**, *312*, 390.
[54] R. Zheng, Z. Wu, Y. Yan, J. Wang, J. Huang, *RSC Adv.* **2015**, *5*, 17253.
[55] D. Duddens, A. Heuer, O. Borodin, *Macromolecules* **2010**, *43*, 2028.
[56] R. Xue, Y. Han, Y. Xiao, J. Huang, B-Z, T. , Y. Yan, *ACS Appl. Nano Mater.* **2018**, *1*, 122.
[57] K. Chrissopoulou, K. Andrikopoulos, S. Fotiadou, S. Bollas, C. Karageorgaki, D. Christofilos, G. Voyiatzis, S. Anastasiadis, *Macromolecules* **2011**, *44*, 9710.
[58] C. Saujanya, S. Radhakrishnan, *J. Appl. Polym. Sci.* **1996**, *65*, 1127.
[59] H. Tadokoro, Y. Chatani, T. Yoshihara, S. Tahara, S. Murahash, *Macromol. Chem. Phys.* **1963**, *73*, 109.
[60] H. Wang, J. Keum, A. Hiltner, E. Baer, B. Freeman, A. Rozanski, A. Galeski, *Science* **2009**, *323*, 757.
[61] K. Liu, Y. Song, W. Feng, N. Liu, W. Zhang, X. Zhang, *J. Am. Chem. Soc.* **2011**, *133*, 3226.
[62] J. Tellis, C. Strulson, M. Myers, K. Kneas, *Anal. Chem.* **2011**, *83*, 928.